JOURNAL OF GEOPHYSICAL RESEARCH: ATMOSPHERES, VOL. 118, 6651–6662, doi:10.1002/jgrd.50522, 2013

Gas/particle partitioning of total alkyl nitrates observed with TD-LIF in Bakersfield

A. W. Rollins,[1,2] S. Pusede,[1] P. Wooldridge,[1] K.-E. Min,[2,3] D. R. Gentner,[4] A. H. Goldstein,[4,5] S. Liu,[6] D. A. Day,[6,7] L. M. Russell,[6] C. L. Rubitschun,[8] J. D. Surratt,[8] and R. C. Cohen [1,3]

Received 27 February 2013; revised 30 April 2013; accepted 27 May 2013; published 26 June 2013.

[1] Limitations in the chemical characterization of tropospheric organic aerosol (OA) continue to impede attempts to fully understand its chemical sources and sinks. To assess the role of organic nitrates in OA, we used a new thermal dissociation-laser induced fluorescence-based (TD-LIF) technique to obtain a high-time-resolution record of total aerosol organic nitrates (hereafter ΣANs_{aer}) at the Bakersfield, CA supersite during the 2010 CalNex campaign. The TD-LIF measurements compare well with Fourier transform infrared measurements from collocated filter samples. These measurements show that ΣANs are a ubiquitous component of the OA with the $-ONO_2$ subunit comprising on average 4.8% of the OA mass. Scaling this fraction by an estimate of the organic backbone mass yields an estimate that 17–23% of OA molecules contain nitrate functional groups. Measurements of both total ΣAN (gas + aerosol) and ΣAN_{aer} show that on average 21% of ΣANs are in the condensed phase, suggesting atmospheric organic nitrates have similar volatilities to analogous non-nitrate oxidized organic compounds. The fraction of ΣAN that is in the condensed phase increases with total OA concentration, providing direct evidence from the atmosphere that absorptive partitioning into OA has some control over the ΣAN phase partitioning. The specific molecular identity of the ΣAN is incompletely understood. Both biogenic hydrocarbons and long chain alkanes are calculated to be significant sources of low volatility nitrates in Bakersfield, and ultra performance liquid chromatography coupled to an electrospray ionization high-resolution quadrupole time-of-flight mass spectrometer measurements confirm the existence of particulate nitrooxy organosulfates derived from gas-phase oxidation of both isoprene and monoterpenes.

Citation: Rollins, A. W., et al. (2013), Gas/particle partitioning of total alkyl nitrates observed with TD-LIF in Bakersfield, *J. Geophys. Res. Atmos.*, *118*, 6651–6662, doi:10.1002/jgrd.50522.

1. Introduction

[2] Attempts to predict the relationships between ambient secondary organic aerosol (SOA) concentrations and SOA precursor emissions continue to be challenged in part by limitations in the chemical characterization of organic aerosol (OA). Laboratory experiments have measured aerosol mass yields that result from the oxidation of several organic compounds typically found in the atmosphere [*Hallquist et al.*, 2009], and ambient aerosol has been extensively analyzed with hundreds of molecules being identified [*Williams et al.*, 2010]. However, in the best cases, no more than ~15% of the mass of ambient OA has been specifically identified, thereby limiting our ability to directly assign specific SOA precursors and reaction pathways.

[3] Recently, functional group and mass spectral analyses of whole aerosol have provided considerable insight into SOA sources and chemistry [*Jimenez et al.*, 2009; *Russell et al.*, 2011]. Despite this progress, the links between specific gas-phase precursors and aerosol concentrations and properties remain tenuous, and several gaps in our understanding are prominent: (1) the role of anthropogenic NO_x emissions in controlling SOA mass and properties is not clearly

Additional supporting information may be found in the online version of this article

[1]Department of Chemistry, University of California, Berkeley, California, USA.
[2]Now at NOAA Earth System Research Laboratory, Chemical Sciences Division and CIRES, Boulder, Colorado, USA.
[3]Department of Earth and Planetary Sciences, University of California, Berkeley, California, USA.
[4]Department of Civil and Environmental Engineering, University of California, Berkeley, California, USA.
[5]Department of Environmental Science Policy, and Management, University of California, Berkeley, California, USA.
[6]Scripps Institution of Oceanography, University of California, San Diego, La Jolla, California, USA.
[7]Now at CIRES, University of Colorado Boulder, Boulder, Colorado, USA.
[8]Department of Environmental Sciences and Engineering, University of North Carolina at Chapel Hill, Chapel Hill, North Carolina, USA.

Corresponding author: R. C. Cohen, Department of Chemistry, University of California, Berkeley, CA 94720 USA. (rccohen@berkeley.edu)

2169-897X/13/10.1002/jgrd.50522

understood [*Hoyle et al*., 2011], (2) observations that provide a clock for understanding aerosol time evolution show that typically OA is more oxidized than is consistent with gas-phase oxidation rates and mechanisms [*Dzepina et al*., 2011; *Hodzic et al*., 2010], (3) correlations between OA and chemical tracers indicate SOA has an anthropogenic origin, yet ^{14}C measurements indicate that the carbon in OA is largely biogenic [*Weber et al*., 2007], and (4) the generally accepted microphysical model of OA is one that assumes organic particles are liquid and that the hundreds to thousands of compounds in that liquid act as a solvent into which individual molecules partition on the basis of their saturation vapor pressure according to Raoult's law [*Donahue et al*., 2006; *Pankow*, 1994; *Robinson et al*., 2007]. While many laboratory observations support the equilibrium partitioning model, some observations suggest aerosol particles are solid or glassy and thus that gas-aerosol equilibration time scales would be too slow to be the basis for atmospheric modeling [*Cappa and Wilson*, 2011; *Koop et al*., 2011]. Additionally, several studies indicate that many SOA compounds are not inert in the condensed phase, and therefore gas-phase chemistry combined with gas/particle equilibrium cannot capture the complete dynamics of SOA processes [*Kroll et al*., 2009; *Lim et al*., 2010].

[4] Understanding the role of organic nitrate ($RONO_2$) functional groups in OA can shed light on these issues. Aside from minor primary sources of short chain nitrates that do not contribute to OA (e.g., methyl nitrate), $RONO_2$ is primarily a result of oxidation of organic compounds in high-NO_x environments, providing a unique tracer for SOA produced in anthropogenic plumes [*Weber et al*., 2007]. Nitrate functional groups are primarily derived from anthropogenic emissions of nitric oxide (NO); thus, aerosol that incorporates these groups will correlate with tracers of anthropogenic emissions even if the carbon backbone is biogenic [*Perring et al*., 2013].

[5] In the laboratory, oxidation of medium-sized (C_5–C_9) organic molecules that are important in the atmosphere shows that chemical production of alkyl and multifunctional nitrates forms aerosol in moderate yields for chemistry initiated by both the NO_3 radical [*Ng et al*., 2008; *Rollins et al*., 2009] and by OH [*Lim and Ziemann*, 2005; *Matsunaga and Ziemann*, 2008]. In many chamber studies, high-NO_x conditions and therefore $RONO_2$ formation suppress the higher yields of alternative aerosol formation mechanisms [*Kroll et al*., 2006; *Ng et al*., 2007]. For C_{10} and larger molecules, chamber observations and structure-activity relationships [*Pankow and Asher*, 2008] indicate that adding $–ONO_2$ functional groups reduces the vapor pressure of the reaction products to a point where they partition significantly into the condensed phase and two or more oxygen-containing functional groups put the molecules almost exclusively in the condensed phase.

[6] In contrast to these laboratory observations, for ambient aerosol, it has been difficult to characterize the role of $–ONO_2$ functional groups. Many traditional techniques and some state-of-the-art methods for aerosol analysis are generally unable to discriminate between organic and inorganic nitrate (e.g., NO_y detection and aerosol mass spectrometers). However, recent applications of chemical instrumentation including Fourier transform infrared (FTIR), liquid chromatography/electrospray ionization-mass spectrometer (LC/ESI-MS), ESI-MS, and aerosol mass spectrometer (AMS) have established the importance of multifunctional organic nitrates in atmospheric OA [*Day et al*., 2010; *Farmer et al*., 2010; *Nguyen et al*., 2011; *O'Brien et al*., 2013; *Surratt et al*., 2008].

[7] Here we apply a new technique that uniquely detects aerosol organic nitrate. We observe the total of gas and particulate $RONO_2$ (ΣAN) using thermal dissociation-laser-induced fluorescence (TD-LIF), and simultaneously the particle only $RONO_2$ (ΣAN_{aer}) using TD-LIF in combination with a gas-phase denuder [*Rollins et al*., 2010]. The measurements are made with high-time resolution (~5 min) allowing us to examine the variability in aerosol composition on the time scales of fluctuations in source composition and chemistry. In a recent publication [*Rollins et al*., 2012], we discussed nighttime observations that demonstrate the importance of nitrate radical chemistry as a SOA source. In this work, we use the daytime observations to observe the OA mass (C_{OA}) dependence of the $RONO_2$ partitioning into aerosol in the atmosphere and to constrain the saturation concentration (C^*) distributions of the ambient nitrates.

2. Measurements

2.1. CalNex SJV Site

[8] The measurements reported here were collected at the CalNex 2010 San Joaquin Valley (SJV) site in Bakersfield California during 15 May to 29 June 2010. Bakersfield is located at the southern end of the SJV, which is one of the most productive agricultural regions in the United States. The region has extensive lands devoted to cattle raising and active oil and natural gas drilling and processing industries. The CalNex SJV site was located at 35.3463°N –118.9654°W, which is approximately 6 km southeast of the Bakersfield city center. A busy commuter freeway lies 0.75 km to the north of the site. The prevailing winds in the morning were typically from the southwest at ~5 km/h. Throughout the day the winds gradually increased and shifted to the northwest with an average daily maximum speed of 15 km/h [*Ahlm et al*., 2012]. A map of the SJV and location of the measurement site with typical daytime wind direction is shown in Figure 1.

2.2. TD-LIF Instruments

[9] Measurements of ΣAN and ΣAN_{aer} were conducted using TD-LIF [*Day et al*., 2002; *Wooldridge et al*., 2010]. This was the first field deployment of the ΣAN_{aer} measurement [*Rollins et al*., 2010]. The TD-LIF instruments detect ΣAN by sampling air through a heated quartz inlet tube into an LIF-based NO_2 detector. The inlet temperature is typically held near 320°C where all organic compounds of the form $RONO_2$ decompose in the gas phase quantitatively yielding $RO + NO_2$. The specifics of the system used in this study to make the ΣAN measurements are described by *Day et al*. [2002], and an intercomparison with independent measurements of speciated gas-phase $RONO_2$ is described by *Beaver et al*. [2012].

[10] The ΣAN_{aer} measurements were made using the instrument described in *Rollins et al*. [2010]. In this instrument, LIF of NO_2 was accomplished by excitation at 408 nm using a 30 mW single-mode continuous-wave diode laser (Power Technology). Red-shifted fluorescence photons were detected at wavelengths long of 650 nm using a photomultiplier tube

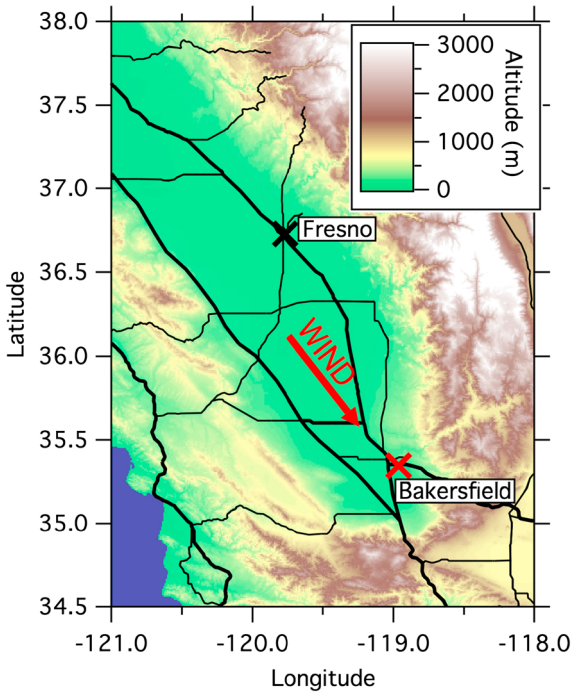

Figure 1. Map of San Joaquin Valley. Black lines show interstates and major highways. Red × shows CalNex SJV measurement site in SE Bakersfield. Typical midday wind direction is indicated.

module (Hamamatsu H7421-50). Scattered photons were filtered from the signal using a stack including one each colored glass (Schott) and dielectric (Barr) 650 nm long pass filters. A 38 pass White Cell, identical to that used in *Thornton et al.* [2000], was employed to achieve the desired signal:noise, which typically resulted in a 19 pptv detection limit for one minute of averaging.

[11] The ΣAN_{aer} instrument uses an activated carbon denuder (MAST Carbon, U.K.) to remove gas-phase NO_y ($NO_y = NO + NO_2 + NO_3 + RONO_2 + 2 \times N_2O_5 + ClNO_2 + \ldots$) from the sample flow before entering the heated section of the inlet, where particles are evaporated and $RONO_2$ is converted quantitatively to NO_2. The difference between the instrument used here and that described by *Rollins et al.* [2010] is primarily in the denuder used to remove gas-phase NO_y. For this study, we used a more efficient multichannel denuder that was 2.2 cm in diameter and 10 cm long (MAST Carbon, UK). The channels comprised 44% of the cross-sectional area of the denuder, which with the 500 sccm flow rate resulted in a transit time of 1.9 s through the denuder. At ambient temperatures, this resulted in an insignificant evaporative loss of semivolatile particles. A dry $PM_{2.5}$ cyclone was used to remove large particles before air entered the denuder. An automated stainless steel ball valve (Swagelok) was used to periodically bypass the denuder and flow NO_2 calibration standards into the instrument. Measurements of the instrument's zero response were made by overflowing the inlet through the denuder with zero air. Both the zero and calibration constants had regular diurnal variations on the order of 10% due to changes in laser alignment resulting from temperature changes in the trailer that housed the instruments. Measurements of the instrument's calibration constant were performed hourly and zero measurements every 30 min. These were sufficient to observe all significant variations in the instrumental characteristics and maintain high accuracy without significantly reducing the duty cycle (duty cycle ~90%).

[12] The TD-LIF inlets were located on a scaffold tower with the ΣAN_{aer} inlet at 5.5 m above ground level, and the ΣAN inlet at 15 m. During the day, observed gradients in NO_2 between the two heights were small, while at night, the two heights often sampled distinct air masses with 10–20% higher NO_2 aloft. At each inlet, the sample flow passed through a critical orifice that reduced the pressure to <60 hPa. The transit time from that point through 3.2 mm ID tubing to the detector is less than 10 ms, keeping the potential for chemistry to affect NO_2 before detection to a minimum [*Wooldridge et al.*, 2010].

[13] The accuracy of the TD-LIF measurement of ΣAN_{aer} is determined by the efficiency of the removal of gas-phase NO_y compounds, the transfer function for particles through the denuder and into the heater, the efficiency with which particulate nitrates are converted to NO_2, and the accuracy of the NO_2 measurement. These issues are discussed in detail by *Rollins et al.* [2010]. Of most concern, is evaporative loss of particles in the denuder. To constrain this term, we calculate the upper limit to evaporative loss assuming evaporation without condensation. Compared to our original work where we used a denuder residence time of 9.3 s for this calculation, here we set the residence time to 1.9 s by a combination of denuder and flow rate. This is sufficiently long to fully remove gas-phase NO_y and reduce the potential evaporation of aerosol by an additional factor of 4.9 [*Rollins et al.*, 2010]. Using the transmission efficiency reported in *Rollins et al.* [2010, supporting material] and the SMPS measurements of the size distribution of the aerosol at Bakersfield, we calculate a mean transmission efficiency through our inlet of 93% (the 7% loss is due to thermophoretic deposition at the heater entrance), and a transmission of better than 90%, for more than 7/8 of the measurements during CalNex.

[14] Mixing ratios of NO_2 resulting from the thermal decomposition of $RONO_2$ are converted to mass concentrations of the nitrate functional group in air using the number density of air and the molecular weight of the nitrate group (62 g mol^{-1}). At standard conditions (1013 hPa, 298 K), this factor is 2.53 μg m^{-3} ppb^{-1}. The instrument typically had a background count rate near 500 counts per second (CPS) due to scatter of laser light in the LIF cell and a sensitivity to NO_2 of 150 CPS ppb^{-1}. For one minute of measurement, this results in a theoretical detection limit (1σ noise at a concentration of zero, [*Thornton et al.*, 2000]) of 0.019 ppb. Concentrations at the site were low; thus, the distribution of differences between adjacent points in the time series (ppb at time $t+1$ min – ppb at t) for all data is expected to be a normal distribution with an approximate width (2σ) of 0.038 ppb. A Gaussian fit to the distribution has a width of 0.0395 ppb, in good agreement with the expected noise level. Converting this measurement of mixing ratio to mass of particulate ΣAN gives a detection limit of 48 ng m^{-3}.

[15] A potential interference for the TD-LIF ΣAN_{aer} measurement is particulate peroxy nitrates (PNs), which would also be detected. These compounds are not expected to contribute significantly to particulate concentrations since their short thermal decomposition lifetime should result in rapid

losses in the condensed phase. For example at 300 K and 1013 hPa in the gas phase, the lifetime of peroxyacetyl nitrate (PAN) to decomposition is 22 min. For particle phase PNs, this lifetime would be expected to be an upper limit due to the absence of NO_2 with which gas-phase PAN exists in equilibrium and the more rapid thermal transfer in the condensed phase which may further decrease PN lifetimes.

[16] A primary advantage of TD-LIF is that ammonium nitrate (NH_4NO_3) is not detected by the instrument due to the significantly higher enthalpy change for the thermal decomposition of HNO_3 (206 kJ mol^{-1}) as compared to $RONO_2$ (e.g., 151 kJ mol^{-1} for CH_3ONO_2, [*Gray et al*., 1981]). Laboratory tests have shown the instrument to be insensitive to NH_4NO_3 when the inlet is held near 320 °C as was done here. The measurements from Bakersfield yield confidence in this as ΣAN_{aer} was more highly correlated to OA than it was to aerosol $NO_3^{(-)}$ even though aerosol $NO_3^{(-)}$ was typically ~10 times ΣAN_{aer} (see Figure 5 and section 4).

2.3. Additional Particle Measurements

[17] Measurements of PM_1 OA concentrations were made using an Aerodyne high-resolution time of flight AMS as described in *Liu et al*. [2012a]. Measurements of organic functional groups including $RONO_2$ were made by FTIR analysis of filter samples [*Day et al*., 2010; *Liu et al*., 2012a]. Typically, FTIR organanitrate group mass has been reported to include the associated fraction of C mass (6 g mol^{-1} of C for a total of 68 g mol^{-1} for organonitrate), but here, all TD-LIF and FTIR organonitrate group mass are reported using 62 g mol^{-1} for consistency. Both (dried) PM_1 and $PM_{2.5}$ samples were collected using FTIR, and typically 83% of the $PM_{2.5}$ $RONO_2$ mass was found to be in PM_1. Both the AMS and filter samplers used inlets on the top of a trailer located next to the sampling tower at the same height as the TD-LIF ΣAN_{aer} measurements. Volatile and intermediate volatility organic compound (VOC, IVOC) measurements on the tower were made by gas chromatography with mass spectral and flame ionization detection [*Gentner et al*., 2012].

[18] A number of isoprene and monoterpene oxidation products in the condensed phase were measured using ultra performance liquid chromatography coupled to an electrospray ionization high-resolution quadrupole time-of-flight mass spectrometer (UPLC/(-)ESI-Q-TOFMS) operated in the negative (–) ion mode [*Surratt et al*., 2008]. Many of the measured compounds were nitrooxy organosulfates. Details of UPLC/(-)ESI-Q-TOFMS operating conditions and procedures can be found elsewhere [*Zhang et al*., 2011]. High-volume filter samplers operating at 226 L min^{-1} with $PM_{2.5}$ inlets were used to collect fine aerosol onto prebaked 86 cm^2 quartz fiber filters. The samples were collected daily from 12 A.M. to 11 P.M. (local time), resulting in 38 individual 23 h filter samples. Field blanks were collected weekly by placing prebaked quartz fiber filters into samplers for 15 min before removing and storing in the same manner as the $PM_{2.5}$ filter samples. All UPLC/(-)ESI-Q-TOFMS filter samples collected during the campaign were shipped frozen to the laboratory. Upon arrival to the laboratory, all samples were stored in a freezer at –18 °C until time of analysis. Before UPLC/(-)ESI-Q-TOFMS analyses, filter samples were extracted using the detailed procedures outlined in Zhang et al. [*Zhang et al*., 2012]. Field and lab blanks were treated similarly to the $PM_{2.5}$ filter samples. No OA constituents detected from the $PM_{2.5}$ filter samples were seen in these blanks, indicating that nitrooxy organosulfates detected by this technique were not introduced during sample storage or preparation.

[19] Nitooxy organosulfates derived from isoprene and monoterpenes were identified based on comparison to prior work by Surratt et al. [*Surratt et al*., 2008]. Specifically, retention times, accurate mass data, and MS/MS spectra were used to confirm the identity of these compounds. None of the nitrooxy organosulfates detected in the $PM_{2.5}$ samples have commercially available standards for quantification. As a result, calibration curves of propyl sulfate (City Chemical, 98% purity), octyl sulfate (Sigma, 99% purity), and decyl sulfate (Fluka, 99% purity) were generated for use as surrogate standards. These three compounds all contained an organosulfate group ($R\text{-}OSO_3$); therefore, their response factors during UPLC/(-)ESI-HR-Q-TOFMS analyses were assumed to be similar to those of the measured nitrooxy organosulfates derived from BVOC oxidation. One of these surrogate standards was chosen to quantify the observed nitrooxy organosulfates from Bakersfield on the basis of retention time and structural similarity (i.e., similar carbon numbers). The approximate identified organonitrate mass from the UPLC/(-)ESI-Q-TOFMS analyses was calculated by scaling the derived organic mass by the mass of the nitrate functional group/compound MW. Significant uncertainties are associated with quantification of these compounds using UPLC/(-)ESI-Q-TOFMS due to variable response factors depending on the compound and the solvents present during ESI analysis [*Cech and Enke*, 2001; *Surratt et al*., 2008].

3. Comparison of Particle $RONO_2$ Measurements

[20] A unique aspect to the instrumentation at the CalNex SJV was that three independent techniques were used for simultaneous measurements of particulate organic nitrates. The PM_1 FTIR samples were typically collected for between 3 and 6 h each. $PM_{2.5}$ samples used for UPLC/(-)ESI-Q-TOFMS analyses were collected for 23 h (12 A.M. – 11 P.M.). TD-LIF measurements were collected at 1 Hz and typically above the detection limit for a 1 min average. All three data sets averaged to the UPLC/(-)ESI-Q-TOFMS time resolution are shown in Figure 2. The total mass of particulate organonitrate measured by UPLC/(-)ESI-Q-TOFMS mass is of order 1% of the other two due to the unavailability of available authentic standards and inability to ionize nonacidic organonitrate constituents. Nonetheless, the UPLC/(-)ESI-Q-TOFMS measurements were somewhat correlated to ΣAN_{aer} ($r = 0.36$), indicating that the measured compounds are representative of important ΣAN_{aer} sources.

[21] Figure 3 shows the TD-LIF measurements averaged to the FTIR time resolution and regressed against the FTIR data. For this comparison, we have adjusted the TD-LIF data down by a factor of 0.83 to adjust for size cut differences between the instruments ($RONO_2$ $PM_1/PM_{2.5}$ [*Liu et al*., 2012a]). A linear fit to the data yields an offset of 0.068 μg/m^3 and a slope of 1.38 (i.e., slope implies FTIR is 28% below TD-LIF). A good correlation was observed ($r = 0.72$); however, Figure 3 shows that the TD-LIF instrument almost always measured more ΣAN_{aer} than the FTIR. The cause(s)

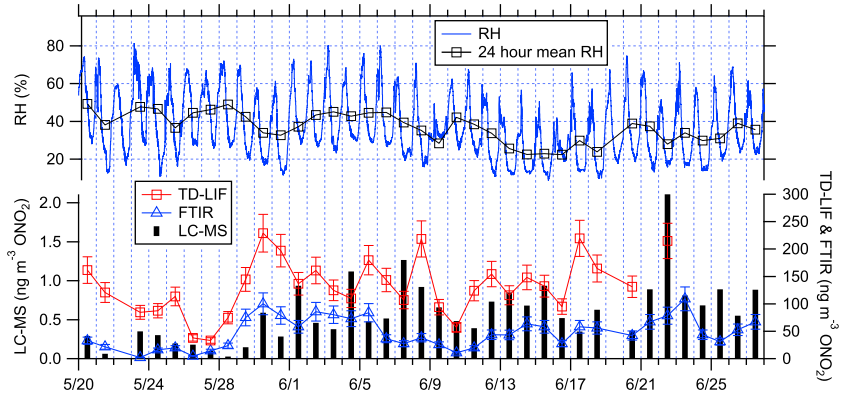

Figure 2. (top) Relative humidity. (bottom) Daily mean particulate $RONO_2$ measured by (black, left axis) LC-MS, (blue, right axis) FTIR, and (red, right axis) TD-LIF. Error bars show accuracy uncertainty ($\pm 2\sigma$) for FTIR and TD-LIF. TD-LIF $PM_{2.5}$ measurements have been scaled down here by a factor of 0.83 for comparison to FTIR PM_1, as described in the text.

of the differences are not obvious, and both research groups rechecked their calibration and other possible sources of positive or negative bias. For the TD-LIF instrument because of the presence of exceptionally high levels of NH_3 and NH_4NO_3 in Bakersfield, we rechecked and confirmed that the instrument is insensitive to these compounds. For the FTIR measurement, samples were dried and frozen, then analyzed 1–2 months later at moderate humidity (<40%). Evaporative loss of nitrates from the filters prior to FTIR analysis is known to occur to some degree, and is challenging to quantify [*Day et al.*, 2010; *Liu et al.*, 2012b]. Due in part to these recognized challenges in these measurements, the stated uncertainty is 20%. The observed difference of 28% would represent losses that are somewhat higher than expected, although the FTIR OA was also 30% below the AMS OA. Comparisons of the FTIR 24 h samples and integrated 3–6 h samples provide evidence that significant losses are not associated with longer sampling times [*Day et al.*, 2010]. Despite the measurement differences, the comparison between the two data sets provides good evidence that both techniques quantify ΣAN_{aer} and puts bounds on the absolute concentration that are of order ±25% from the mean of the two measurements.

4. ΣAN_{aer} Observations

[22] The TD-LIF measurements show that ΣAN_{aer} is an important fraction of both ΣAN and OA. In Figure 4, daytime measurements of ΣAN_{aer} are plotted against ΣAN (10 min means). The linear fit to this data (r = 0.43) shows that during the day, on average 21% of ΣAN is in the particle phase, although there is real variability in this fraction that exceeds the precision of the measurements and is likely due to variations in the chemical identity of the ΣAN molecules. Finding 21% in the condensed phase provides insight into the volatility distribution of the large group of organic compounds comprising ΣAN. As a point of reference, given the typical OA concentrations observed in Bakersfield (~5 μg m^{-3}), compounds existing in the condensed phase via absorptive partitioning must have vapor pressures (P_{vap}) lower than ~10^{-4} Pa. Only very large (~C_{15} and larger) monofunctional nitrates are expected to have vapor pressures this low. As a rough estimate, vapor pressures are reduced by a factor of 100 by the addition of hydroxyl or carbonyl groups [*Pankow and Asher*, 2008], and thus given one to two additional functional groups, nitrates with 5–10 carbon are expected to be found in SOA. Given that almost all of the molecules comprising ΣAN are expected to have less than 15 carbon atoms (See section 5 and Figure 6), this is strong evidence that a large fraction of the organic nitrates in Bakersfield contain two to three oxygen-containing groups and are likely products of two to three oxidation reactions.

[23] In Figure 5, comparisons of ΣAN_{aer} to the AMS PM_1 measurements are shown. Of the aerosol chemical components measured in Bakersfield, we find that ΣAN_{aer} is correlated the most strongly with the AMS OA (r = 0.58). This suggests that ΣAN_{aer} has a similar source to that of other OA, which at this site is dominated by SOA from gas-phase oxidation primarily of anthropogenic VOCs [*Liu et al.*, 2012a]. The correlation with inorganic nitrate (r = 0.43) and with the inorganic ion balance

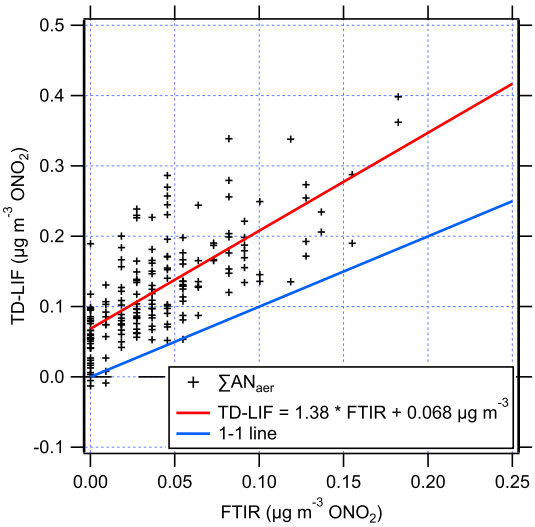

Figure 3. $RONO_2$ measurements by TD-LIF and FTIR. TD-LIF measurements were averaged to FTIR time resolution (3–6 h per data point). Blue line shows 1-1. Red line shows linear least squares fit: TD-LIF = 0.068 μg m^{-3} + 1.38 × FTIR.

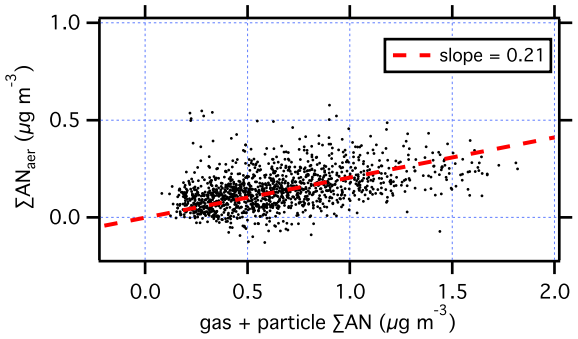

Figure 4. 10 min measurements of particulate alkyl nitrates vs. total alkyl nitrates. A linear fit to the data with the y-intercept fixed at zero (red line) yields a slope of 0.21, or on average 21% of alkyl nitrates in condensed phase.

(molar ratio of 2 × $SO_4^{(2-)} + NO_3^{(-)} + Cl^{(-)}$ / $NH_4^{(+)}$, r = 0.06), a surrogate for particle acidity, was weaker. These observations differ from those of *Day et al.* [2010] who reported observations in coastal southern California with important source regions identified as Riverside and the South Coast Air Basin. Those measurements showed strong correlations between ΣAN_{aer} and inorganic $NO_3^{(-)}$ as well as with the product of AMS organics and $NO_3^{(-)}$ suggesting that similar conditions favored the formation of ΣAN_{aer} and inorganic particulate nitrate. The observed relationships between ΣAN_{aer} and inorganic aerosol compounds may differ between this work and that of *Day et al.* [2010] for multiple reasons. One possibility is that heterogeneous chemistry plays different roles in controlling ΣAN_{aer} in the two locations. The ammonia in Bakersfield was quite high, and consequently Figure 5 shows that the particles were almost always neutralized (molar ion ratio typically ≤1), whereas the observations by *Day et al.* [2010] show this ratio typically greater than 1. Although acidic aerosol was reported to be correlated with low ΣAN_{aer} by *Day et al.* [2010], this was not the case in Bakersfield, and thus acid-catalyzed hydrolysis does not appear to be an important process controlling ΣAN_{aer} content for the majority of the aerosol that were observed in this work. The generally low RH in Bakersfield (nighttime mean high, 60%, daytime mean low, 21%, Figure 8) as compared to source regions in that study (nighttime mean high, 70%, daytime mean low, 45%) may play a role in reducing the importance of nitrate hydrolysis. This argument may be supported by a weak anticorrelation between RH and ΣAN_{aer} observable in Figure 2 although the relationship between RH and ΣAN_{aer} was not consistent enough for us to draw a strong conclusion in this regard. Other possibilities are differences in chemical regime associated with different correlations between VOC and NO_x or absolute levels of VOC and NO_x in the two locations.

[24] On average, in Bakersfield, the ΣAN_{aer} mass (nitrate fragment only) was 4.8% of OA. Given the difference between TD-LIF and FTIR ΣAN_{aer} (TD-LIF 38% higher) the nitrate mass fraction could be as low as 3.5% of PM_1 OA (AMS OA uncertainties are also ± 30% and not considered here). If we assume a molecular weight of the ΣAN_{aer} of 300 g-mol^{-1} (See section 5 and Figure 7), then this translates to 17–23% of the OA mass assigned to molecules with an $-ONO_2$ subunit.

5. ΣAN_{aer} Sources Molecules

[25] The large fraction of OA that is organic nitrate molecules implies that understanding the chemical sources of ΣAN_{aer} will shed light on the sources of OA and provide some indication of the effectiveness of possible strategies for reducing SOA. As an extreme, one can speculate that eliminating the source of ΣAN_{aer} would result in reducing OA by at least 17%. Such a reduction could come about either by eliminating the NO_x that is incorporated into the organic molecules that form the OA or by eliminating the organic precursors. To assess the potential for such strategies, we need more detailed knowledge of the molecular composition of ΣAN_{aer}. While the TD-LIF and FTIR measurements do not provide such information, we can combine the insight from the specific measurements of molecular constituents in the SOA from the UPLC/(-)ESI-Q-TOFMS with a calculation of AN formation rates and P_{vap} based on the observed VOC at the Bakersfield site.

[26] Alkyl and multifunctional nitrates in a continental location such as Bakersfield have essentially no primary sources. The weak sources associated with intercontinental transport of directly emitted nitrates carry molecules with vapor pressures that are too high to be incorporated into aerosol (e.g., methyl nitrate). Therefore, ΣAN_{aer} is likely to only have local sources from gas-phase oxidation of locally

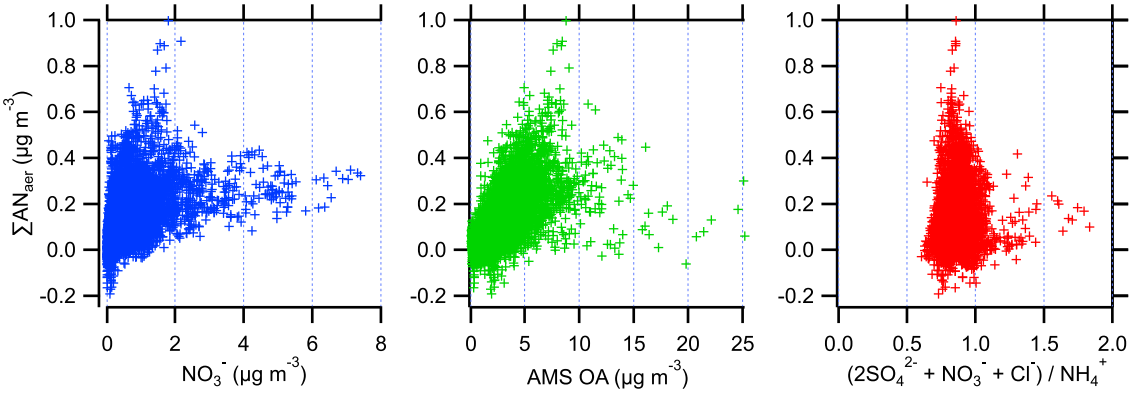

Figure 5. Correlation of pΣAN to (left) inorganic NO_3^- (r = 0.43), (middle) PM1 (r = 0.58), (right) PM1 acidity (r = 0.06). TD-LIF data were averaged onto AMS time resolution, about 5–6 min.

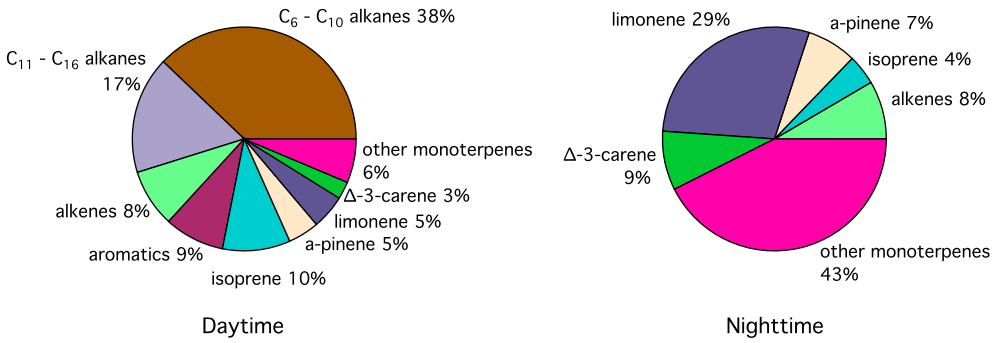

Figure 6. Calculated relative importance of various VOCs to instantaneous ΣAN production. Alkanes with less than six carbons have been omitted from this figure for clarity due to their relatively low importance for SOA formation. Left pie shows distribution of $RONO_2$ formed during the day from $RO_2 + NO$ reaction. Right shows distribution during the night from alkene + NO_3 reactions.

emitted VOCs, involving multigeneration chemistry that results in adding functional groups to a nitrate or a nitrate group to a functionalized molecule [e.g., *Rollins et al.*, 2009], and possibly from chemistry in the condensed phase such as nitration of epoxides in acidic conditions [*Eddingsaas et al.*, 2010; *Hu et al.*, 2011]. Aqueous-phase chemistry may also result in hydrolysis of organic nitrates converting the nitrogen to HNO_3 [*Roberts*, 1990; *Hu et al.*, 2011; *Liu et al.*, 2012b].

[27] In the gas phase, nitrates are produced by oxidation of organic molecules in the presence of NO_x. During the day, the primary source is the reaction of photochemically produced organic peroxy radicals (RO_2) with NO, which can result in the formation of a nitrate, or an organic oxy radical and NO_2.

$$RO_2 + NO \rightarrow RONO_2 \quad \text{(R1a)}$$

$$\rightarrow RO + NO_2 \quad \text{(R1b)}$$

[28] In the presence of oxygen, channel R1b will be followed either by a reaction with O_2 resulting in carbonyl formation,

$$RO + O_2 \rightarrow R = O + HO_2 \quad \text{(R2)}$$

or an intermolecular isomerization or decomposition. During nighttime, sources of hydroxyl radicals (OH) are nearly absent, but a significant channel to form $RONO_2$ exists due to the reaction of nitrate radicals (NO_3) with olefins. The yield (α) of $RONO_2$ for a given compound/oxidant combination is the fraction of the $RO_2 + NO$, or $R = R' + NO_3$ reactions which yield $RONO_2$. Through (R1) the yields of $RONO_2$ are low for small organic compounds (a fraction of a percent for CH_3O_2) and increase with carbon number to a limiting yield near 35–40% for C_{8-10} peroxy radicals [*Arey et al.*, 2001; *Atkinson et al.*, 1982; *Carter and Atkinson*, 1989]. Key species in many locations are biogenics, such as isoprene, which has a net yield (multiple $RONO_2$ isomers) of $12\% \pm 3\%$ [*Paulot et al.*, 2009; *Sprengnether et al.*, 2002] and monoterpenes such as α-pinene (~18% yield [*Nozière et al.*, 1999]). Yields for NO_3 initiated oxidation are much higher (>50%), and nighttime production of ΣANs may approach 50% of the daytime production rate [*Fry et al.*, 2013].

[29] We use the VOC measurements in Bakersfield, weighting these by their reactivities towards OH or NO_3, and yields to form AN to calculate an estimate of the relative importance of different primary VOC as chemical sources of ΣAN_{aer}. There is relatively little time of day variation in the calculated daytime or nighttime fractional importance of the AN sources, and thus we show in Figure 6 two pie charts representing the contributions of VOC to production of ΣAN_{aer} initiated by OH (daytime) and NO_3 (nighttime). Tables 1 and 2 in the supporting information provide the details of the calculations. The compounds that are important are not the same compounds that are important to O_3 production or to total OH reactivity.

[30] During the day, the dominant source of nitrates is calculated to be moderate to large anthropogenic alkanes, which are known to have high AN and SOA yields [*Lim and Ziemann*, 2005] and alkenes. Anthropogenic VOC emissions were also concluded by *Liu et al.* [2012a] to be the major SOA source at this site. Terpenes including α-pinene and *d*-limonene are also an important source of nitrates, and these are known to have low P_{vap}. Isoprene was a significant contributor to primary AN production. Multigenerational chemistry has been shown to produce significant SOA from isoprene, and isoprene oxidation products, such as the nitrooxy organosulfates, have also been previously observed in ambient SOA [*Claeys et al.*, 2004; *Surratt et al.*, 2008]. We only include the first generation in these calculations.

[31] The UPLC/(-)ESI-Q-TOFMS data provide additional evidence that monoterpenes and multiply oxidized isoprene products are important to the organic nitrate fraction of the aerosol. A number of specific nitrooxy organosulfates were observed; these included two derived from isoprene oxidation observed at *m/z* 260 ($C_5H_{10}NO_9S^-$) and 305 ($C_5H_9N_2O_{11}S^-$) as well as eight derived monoterpene oxidation observed at *m/z* 294 ($C_{10}H_{16}NO_7S^-$), 296 ($C_9H_{14}NO_8S^-$), 310 ($C_{10}H_{16}NO_8S^-$), 312 ($C_9H_{14}NO_9S^-$),

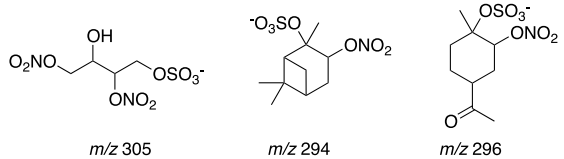

Figure 7. Dominant nitrated ions detected by LC-MS.

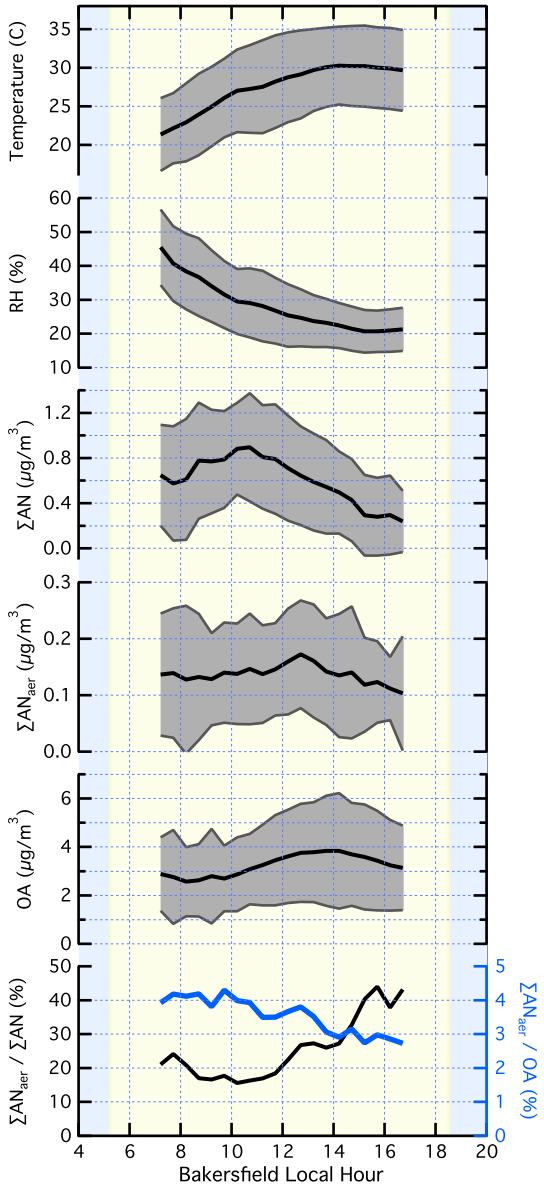

Figure 8. Average diurnal profiles of the data used in the daytime analysis for (from top) ambient temperature, relative humidity, ΣAN, ΣAN_{aer}, and PM_1 OA. In each case, the dark line shows mean, and the shaded region shows the $\pm 1\sigma$ range. Bottom panel shows the ratios (%) of the mean diurnal values ΣAN_{aer} / OA (black, left axis) and ΣAN_{aer} / ΣAN (blue, right axis) Yellow background indicates day (solar zenith angle <85°). The ΣAN_{aer} shown is PM2.5. This value was scaled by 0.83 to calculate PM1 ΣAN_{aer} / OA.

326 ($C_{10}H_{16}NO_9S^-$), 328 ($C_{10}H_{18}NO_9S^-$), 330 ($C_9H_{16}NO_{10}S^-$), 342 ($C_{10}H_{16}NO_{10}S^-$), and 373 ($C_{10}H_{17}N_2O_{11}S^-$). All of these nitrooxy organosulfates can be generated from isoprene and monoterpene oxidation by either OH under high-NO_x conditions or by NO_3, both in the presence of acidified sulfate aerosols [*Surratt et al.*, 2008].

[32] The three most abundant (i.e., *m/z* 305, 294, and 296) of these are shown in Figure 7. Interestingly, these most abundant ions have been demonstrated to form from isoprene (*m/z* 305), α-pinene (*m*/z 294), and *d*-limonene (*m/z* 296) oxidation [*Surratt et al.*, 2008], consistent with their importance to contributing to the AN production shown in Figure 6, especially at night. The total mass of ΣAN_{aer} estimated from the UPLC/(-)ESI-Q-TOFMS observations is on average 0.4% of the TD-LIF ΣAN_{aer}. One reason for the low fraction of ΣAN_{aer} observed by UPLC/(-)ESI-Q-TOFMS is that this technique is only sensitive to organic compounds containing acidic functional groups, such as organosulfates, which efficiently deprotonate during the ESI process and are detected in the negative ion mode as $[M - H]^-$ ions. The exact mechanisms for nitrooxy-organosulfate formation remain unknown [*Surratt et al.*, 2008], but there are no known mechanisms in the gas phase to produce these compounds. These compounds likely form through heterogeneous chemically pathways and warrant further investigation. Due to the low RH and particle acidity in Bakersfield, the aqueous-phase reactions forming sulfates are expected to be slow there, and thus, most of the ΣAN_{aer} molecules probably do not have these groups that make them detectible using this technique. Further, while hydroxynitrates are a significant oxidation product of alkenes, this is not the case for alkanes, and thus this potentially significant subset of ΣAN_{aer} due to alkanes may not be detectable using existing techniques.

6. Gas/Particle Partitioning of ANs

[33] Absorptive partitioning theory based on Raoult's law postulates that the fraction of each organic compound that is found in the condensed phase increases with the mass of absorbing (solvating) aerosol (C_{OA}). For atmospheric organic species, the chemical identity of C_{OA} has been suggested to be total OA. In the case of water-soluble organics, condensed phase liquid water has also been suggested to serve as the solvent. In either case, if absorptive partitioning theory is correct, then the equilibrium fraction of a specific compound found in the condensed phase (Y_i) is described by equation (1).

$$Y_i = \frac{C_{i,p}}{C_i} = \frac{C_{OA}/C_i^*(T)}{1 + C_{OA}/C_i^*(T)} = \left(1 + \frac{C_i^*(T)}{C_{OA}}\right)^{-1} \quad (1)$$

[34] Here, C_i and $C_{i,p}$ are, respectively, the total and particle phase concentrations of species *i*, and $C_i^*(T)$ is the temperature-dependent saturation concentration of species *i*. In this theory, the equilibrium variations in the partitioning of a specific compound are only due to changes in C_{OA} or *T* [*Donahue et al.*, 2006; *Pankow*, 1994].

[35] Figure 8 shows average diurnal profiles of ΣAN, ΣAN_{aer}, AMS OA, ambient temperature, as well as the mass fraction of OA that was nitrate and the fraction of ΣAN in the condensed phase over the time range 15 May to 29 June 2010. We show only the daytime measurements (7 AM – 5 PM) that are used in the following analysis. The observed increase of ΣAN was strongest in morning (8 AM – 11 AM). However, the largest concentrations of ΣAN_{aer} were observed later in the day, coincident with an increase in the total OA. The ΣAN_{aer} contribution to total OA was highest in the early morning and steadily decreased throughout the day. This observation is explained by the differences between nighttime VOC oxidation, which is dominated by nitrate radical leading to high yields of organic nitrates, and photochemistry which generally has

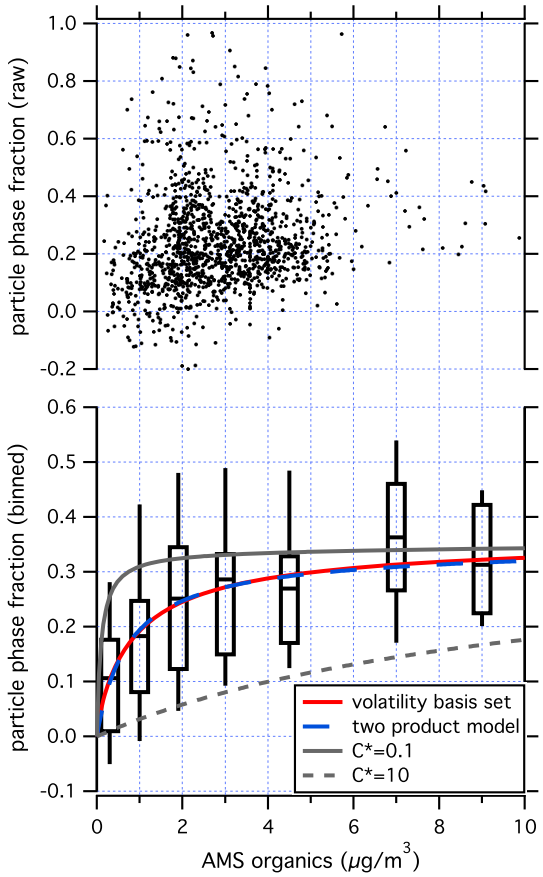

Figure 9. Particle phase fraction of organic nitrates fit to adsorption partitioning theory. Black dots show 10 min averages. Data binned by total OA are shown by box and whiskers. Boxes show means (horizontal bars), 25–70 percentile range (boxes), and 10–90 percentile range (whiskers). Boxes are centered at the average mass value for the data points in each bin. Bins are more closely spaced at lower *OA* values due to the larger number of data points. Two product model and volatility basis set fits both shown. Red line shows the best volatility basis set fit, and blue dashes show two product model fit. To illustrate the significance of fit, solid and dashed gray lines show how the partitioning curve would look if 34% of the OM has $C^* = 0.1$ (upper) and $C^* = 10$, and 66% is completely volatile.

lower yields of ANs [*Rollins et al.*, 2012]. The fraction of ΣAN in the condensed phase increased in the afternoon, indicating decreases in ΣAN volatility and/or partitioning to the condensed phase due to an increase in C_{OA}.

[36] Analysis of the variability in the $\Sigma AN_{aer}/\Sigma AN_{total}$ (Y_{tot}) data indicates that temperature and RH have a weak or nonobservable effect on the gas/particle partitioning of ΣAN over the ranges sampled. In contrast, total OA mass does have an observable influence on Y_{tot}. Larger concentrations of OA are associated with an increase in the fractions of ΣAN in the aerosol phase (Figure 9), as is expected from absorptive partitioning.

[37] To determine the volatility distribution of organic nitrates, we analyze the data assuming absorptive partitioning controls the fraction of ΣAN in the condensed phase. Here we presume that the observed C_{OA} dependence of the fraction of total organic nitrates in the particle phase (pΣAN / ΣAN = Y_{tot}) can be reproduced using a finite number of surrogate compounds of varying C_j^*.

$$Y_{tot} = \frac{\sum_i C_i Y_i}{\sum_i C_i} = \sum_{j=1}^{n} F_j \left(1 + \frac{C_j^*}{C_{OA}}\right)^{-1} \quad (2)$$

[38] We explicitly distinguish the real compounds (i) from surrogate compounds (j). F_j is the fraction of ΣAN that can be represented as having a saturation concentration C_j^* and thus $\sum_{j=1}^{n} F_j = 1$. The two product model for example [*Odum et al.*, 1996] is equivalent to equation (2) where $n = 2$.

[39] Figure 9 shows Y_{tot} (10 min average of ΣAN_{aer} / 10 min average of ΣAN) plotted against M_0 and equation (2) with varying n was used as a fitting function. Because ΣAN is in the denominator of Y_{tot}, the analysis is especially sensitive to noise in this parameter. The ΣAN measurement is made by subtracting the sum of NO_2 and peroxynitrates measured in one instrument channel from the sum of these plus ΣAN measured with another channel [*Day et al.*, 2002]. Therefore, the ΣAN quantity was frequently quite noisy due to very high (>100 ppb) and rapidly changing NO_2. The particle ΣAN channel is much less noisy since NO_2 is removed with the denuder. As a result, ΣAN_{aer} was measured more precisely than ΣAN_{total} even though the concentrations of the aerosol organic nitrate were lower.

[40] Equation 2 has been used throughout the literature to fit data in two different ways. The so-called two product model uses equation (2) with $n = 2$, and both F_j and C_j^* are used as fitting parameters. More recent publications have followed *Donahue et al.* [2006] using the so-called volatility basis set approach where the C_j^* are fixed and logarithmically spaced and only the F_j are used as fitting parameters. Typically, four C^* values have been sufficient to fit the data, and so both methods frequently result in four fitting parameters. We have fit our data with both the two product model and the volatility basis set using various basis sets. Using the two product model, the best-fit parameters were: $F_1 = 0.34$, $C_1^* = 0.73$, $F_2 = 0.66$, $C_2^* > 100$. Here we state C_2^* as having a lower limit of 100 because we cannot constrain an upper on the value of C_2^* given that the OA concentration of our measurements did not significantly exceed 10 μg/m^3. This essentially means that 66% of the organic nitrates are too volatile to condense under any ambient OA loadings in Bakersfield. Using the volatility basis set approach, we tried using basis sets spanning the range 10^{-1} – 10^3. The best fit uses $C_1^* = 0.1$, $F_1 = 0.04$, $C_2^* = 1$, $F_2 = 0.30$, $C_3^* > 100$, $F_3 = 0.66$. Both fitting approaches are shown in Figure 9, and it is clear that there is virtually no difference in the quality of fit. To illustrate the significance of the fit, we also show in Figure 9 two partitioning curves assuming that 66% of the OM is completely volatile, and the remaining 34% has a single C* value of 0.1 or 10.

[41] The fit to the data in Figure 9 demonstrates that under ambient conditions with moderate OA concentrations, typically ~20% of ANs are in the condensed phase and that at OA concentrations above 10 μg/m^3 as much as 34% will condense. This is significantly more than would be expected from the chemistry captured by a calculation of the distribution of vapor pressures of first generation oxidation products

of the measured AN precursors. To illustrate this point, we used the SPARC model [*Hilal et al*., 2003] to estimate vapor pressures of the nitrates generated from the known sources in Bakersfield as indicated in Figure 6. For each precursor, a representative nitrate product was used to estimate the vapor pressure of the class of products. The SIMPOL model [*Pankow and Asher*, 2008] was also used to calculate vapor pressures for many compounds, and SIMPOL and SPARC agreed within a factor of 2–3. Vapor pressures were converted to C^* values assuming an average MW for OA of 200 g/mol. Using these saturation concentrations, less than 1% of ΣAN is predicted to be in the condensed phase under all observed M_0 conditions. A uniform decrease in vapor pressure of all nitrates of 10^4–10^5 is required to calculate, respectively, 19–28% of the nitrates in the condensed phase at 3 μg/m^3 (a typical OA concentration, Figure 8). This suggests that nitrates have undergone approximately two additional stages of oxidative chemistry beyond the initial VOC + OH reactions. This is of course a gross simplification since we have done the calculation assuming that all compounds are reduced as opposed to increased in volatility through atmospheric oxidation. However, the same result is achieved if we only reduce the volatility of those compounds that start with at least nine carbons (and isoprene). All smaller compounds even after a reduction in vapor pressure by a factor of 10^5 still have C^* values greater than 40 μg/m^3, meaning that they do not significantly contribute to particles. The finding that ~2 generations of oxidative aging are required to explain the observations of AN volatility is in good qualitative agreement with a number of recent studies that have estimated the volatility and age of atmospheric OA [e.g., *Hildebrandt et al*., 2010; *Jimenez et al*., 2009; *Russell et al*., 2011].

7. Discussion and Conclusions

[42] A new technique was used to successfully quantify ambient total particulate organic nitrates with higher time resolution and precision than previously reported techniques. The data compare well with those from colocated FTIR filter measurements.

[43] Nitrates were found to be ubiquitous in the OA in Bakersfield, with on average 4.8% of the mass being from this moiety during the day. Calculations suggest that the most significant sources of the nitrated OA molecules are gas-phase oxidation of both biogenic hydrocarbons and long-chain anthropogenic alkanes. Isoprene and monoterpene oxidation products containing one to two nitrate groups were chemically characterized in the condensed phase using UPLC/(-)ESI-Q-TOFMS, and the dominant compounds from monoterpenes measured had one nitrate group and total molecular weights near 300 amu (Figure 7). For these compounds, the nitrate mass fraction is ~20%. In the case of the detected isoprene oxidation product with two nitrate groups, it had a molecular weight of 306, resulting in a nitrate mass fraction of 40%. If these molecules represent typical nitrated SOA, then we calculate that on the order of 17–23% of OA molecules are organic nitrates.

[44] Bakersfield is a high NO_x environment meaning that almost all organic peroxy radicals produced during the day react with NO, eventually forming either a nitrate, an alcohol, or a carbonyl. Our observation that ~17–23% of SOA molecules contain nitrate groups is comparable to the yields to form nitrates in the gas phase from molecules large enough ($>C_4$) to form SOA (i.e., α, section 5 and Table 2 in SI). This is suggestive that the product channel following the $RO_2 + NO$ reaction does not have a significant control over the SOA yield (i.e., fraction of gas-phase oxidation products that are nitrates ≈ fraction of SOA molecules that are nitrates). This suggests that nitrates have a similar volatility and condensed-phase stability to other SOA forming molecules, a result similar to one we found in a laboratory study [*Rollins et al*., 2010]. This conclusion is consistent with the similar vapor pressure changes expected from the addition of these different functional groups to a molecule [*Pankow and Asher*, 2008]. Thus, our measurements would suggest that if NO_x has a significant impact on photochemical SOA formation in the atmosphere, it is likely due to an acceleration of photochemistry, or fragmentation of hydrocarbon backbones as opposed to which functional group quenches the organic radical. In this work, we did not see evidence that condensed-phase hydrolysis or acidic chemistry played a major role in determining nitrate concentrations.

[45] The simultaneous measurements of ΣAN_{aer} and ΣAN allowed us to observe that the gas/particle partitioning of nitrates is a function of total OA, in agreement with equilibrium partitioning theory. We also observe an additional time of day dependence of $\Sigma AN_{aer}/\Sigma AN$ (Figure 8). Because we could not see a direct relationship between all of the $\Sigma AN_{aer}/\Sigma AN$ and temperature data, we conclude that the diurnal variability in $\Sigma AN_{aer}/\Sigma AN$ is most likely due to chemistry, with increases in this ratio late in the day probably due to the production of more highly oxidized and condensable compounds. These measurements also allowed us to constrain the effective saturation concentration distribution of the nitrates in ambient OA, under the assumption of equilibrium partitioning. Thus far, saturation concentrations for ambient OA have only been quantified indirectly using thermaldenuders [*Cappa and Jimenez*, 2010; *Huffman et al*., 2009; *Lee et al*., 2010]. We find that approximately one third of the nitrates have saturation concentrations on the order of 1 μg/m^3. This is significant because typically OA concentrations in Bakersfield are near this level, and therefore SOA appears to potentially have an important positive feedback on itself in this location.

[46] The results presented here for organic nitrates exhibit strong parallels to those shown by [*Hennigan et al*., 2009] who described gas/particle partitioning of total water-soluble organic compounds (WSOC). On average, *Hennigan et al*. [2009] found that 24% of WSOC was in the condensed phase, compared to our observed 21% of ΣAN being condensed. They observed that the fraction of WSOC in the condensed phase increases with the particulate WSOC ($WSOC_p$), but does not increase with total OC (measured using a Sunset Labs EC/OC analyzer). This suggested that a significant fraction of OC is not soluble in water and that the activity coefficients of WSOC in this nonwater soluble OA deviate significantly from one. Nevertheless, *Hennigan et al*. [2009] observed very similar partitioning behavior with respect to $WSOC_p$ concentrations that we observed for ΣAN with respect to the AMS OA. There, $WSOC_p$ partitioning increased up to $WSOC_p$ concentrations of ~4μg/m^3 above which a plateau was observed, suggesting the C^* values for WSOC are effectively within a factor of 2–3 of those derived

in this work for ΣAN. While *Hennigan et al*. [2009] have observed that high RH and particulate water enhance partitioning of WSOC to the particle phase, we did not observe any trend in ΣAN partitioning with RH. However, this may be only due to the lack of high RH observations in Bakersfield. Very few episodes of RH higher than 70% were observed there, where *Hennigan et al*. [2009] did not see significant enhancements in the partitioning below 70% RH.

[47] The ability to observe total OA mass dependence of ΣAN phase partitioning is a unique aspect of this study. This study and that of *Hennigan et al*. [2009] provide direct evidence (from ambient rather than chamber observations) that absorptive partitioning determines to a significant extent the variability of OA. These observations are challenging to understand in light of recent laboratory studies [e.g., *Cappa and Wilson*, 2011; *Perraud et al*., 2012] that have provided evidence that phase partitioning of atmospheric organic compounds, including nitrates, does not follow equilibrium partitioning theory. We suggest that more targeted laboratory and field observations are needed to fully understand the specific differences between the laboratory explorations of specific chemical systems, and field OA observations. To the extent that equilibrium partitioning does control atmospheric OA, the fact that we observe an increase in particle partitioning with total OA while *Hennigan et al*. [2009] only observed an increase in partitioning with water-soluble OC implies that the activity coefficients of organic compounds in various solvents may play an important and unappreciated role in atmospheric OA formation.

[48] While the chemical environment in Bakersfield is somewhat unique (high NO_x, high NH_x, low RH), it is worth noting that daytime nitrate production in the study region was lower than in many other locations with an effective yield near 2.5% for VOC oxidation. Yields double this value are more typical [*Perring et al*., 2013]. Results from *Fry et al*. [2013] also point out that the organic nitrates are prominent in aerosol, and we look forward to our own and other research teams making observations in distinctly different environments.

[49] **Acknowledgments.** This work is supported by the California Air Resources Board under grants CARB 08-316 and 09-328. E.C.B. was supported by NASA ESSF fellowship.

References

Ahlm, L., et al. (2012), Formation and growth of ultrafine particles from secondary sources in Bakersfield, California, *J. Geophys. Res.*, *117*, D00V08, doi:10.1029/2011JD017144.

Arey, J., S. M. Aschmann, E. S. C. Kwok, and R. Atkinson (2001), Alkyl Nitrate, Hydroxylalkyl Nitrate, and Hydroxylcarbonyl Formation from the NO_x-Air Photooxidations of C_5-C_8 n-Alkanes, *J. Phys. Chem. A*, *105*(6), 1020–1027.

Atkinson, R., S. M. Aschmann, W. P. L. Carter, A. M. Winer, and J. N. Pitts (1982), Alkyl nitrate formation from the nitrogen oxide (NOx)-air photooxidations of C2-C8 n-alkanes, *J. Phys. Chem.*, *86*(23), 4563–4569, doi:10.1021/j100220a022.

Beaver, M. R., et al. (2012), Importance of biogenic precursors to the budget of organic nitrates: Observations of multifunctional organic nitrates by CIMS and TD-LIF during BEARPEX 2009, *Atmos. Chem. Phys.*, *12*(13), 5773–5785, doi:10.5194/acp-12-5773-2012.

Cappa, C. D., and J. L. Jimenez (2010), Quantitative estimates of the volatility of ambient organic aerosol, *Atmos. Chem. Phys.*, *10*(12), 5409–5424, doi:10.5194/acp-10-5409-2010.

Cappa, C. D., and K. R. Wilson (2011), Evolution of organic aerosol mass spectra upon heating: implications for OA phase and partitioning behavior, *Atmos. Chem. Phys.*, *11*(5), 1895–1911, doi:10.5194/acp-11-1895-2011.

Carter, W. P. L., and R. Atkinson (1989), Alkyl nitrate formation from the atmospheric photooxidation of alkanes; a revised estimation method, *J. Atmos. Chem.*, *8*, 165–173.

Cech, N. B., and C. G. Enke (2001), Practical implications of some recent studies in electrospray ionization fundamentals, *Mass Spectrom. Rev.*, *20*(6), 362–387, doi:10.1002/mas.10008.

Claeys, M., et al. (2004), Formation of secondary organic aerosols through photooxidation of isoprene, *Science*, *303*(5661), 1173–1176, doi:10.1126/science.1092805.

Day, D. A., P. J. Wooldridge, M. B. Dillon, J. A. Thornton, and R. C. Cohen (2002), A thermal dissociation laser-induced fluorescence instrument for in situ detection of NO_2, peroxy nitrates, alkyl nitrates, and HNO_3, *J. Geophys. Res.*, *107*(D6), doi:10.1029/2001jd000779.

Day, D. A., S. Liu, L. M. Russell, and P. J. Ziemann (2010), Organonitrate group concentrations in submicron particles with high nitrate and organic fractions in coastal southern California, *Atmos. Environ.*, *44*(16), 1970–1979, doi:http://dx.doi.org/10.1016/j.atmosenv.2010.02.045.

Donahue, N. M., A. L. Robinson, C. O. Stanier, and S. N. Pandis (2006), Coupled partitioning, dilution, and chemical aging of semivolatile organics, *Environ. Sci. Tech.*, *40*(8), 2635–2643, doi:10.1021/es052297c.

Dzepina, K., C. D. Cappa, R. M. Volkamer, S. Madronich, P. F. DeCarlo, R. A. Zaveri, and J. L. Jimenez (2011), Modeling the multiday evolution and aging of secondary organic aerosol during MILAGRO 2006, *Environ. Sci. Technol.*, *45*(8), 3496–3503, doi:10.1021/es103186f.

Eddingsaas, N. C., D. G. VanderVelde, and P. O. Wennberg (2010), Kinetics and products of the acid-catalyzed ring-opening of atmospherically relevant butyl epoxy alcohols, *J. Phys. Chem. A*, *114*(31), 8106–8113, doi:10.1021/jp103907c.

Farmer, D. K., A. Matsunaga, K. S. Docherty, J. D. Surratt, J. H. Seinfeld, P. J. Ziemann, and J. L. Jimenez (2010), Response of an aerosol mass spectrometer to organonitrates and organosulfates and implications for atmospheric chemistry, *Proc. Natl. Acad. Sci. U. S. A.*, *107*(15), 6670–6675, doi:10.1073/pnas.0912340107.

Fry, J. L., et al. (2013), Observations of gas- and aerosol-phase organic nitrates at BEACHON-RoMBAS 2011, *Atmos. Chem. Phys. Discuss.*, *13*(1), 1979–2034, doi:10.5194/acpd-13-1979-2013.

Gentner, D. R., et al. (2012), Elucidating secondary organic aerosol from diesel and gasoline vehicles through detailed characterization of organic carbon emissions, *Proc. Natl. Acad. Sci. U. S. A.*, *109*(45), 18,318–18,323, doi:10.1073/pnas.1212272109.

Gray, P., J. F. Griffiths, and K. Hasegawa (1981), Nonisothermal decomposition of methyl nitrate: Anomalous reaction order and activation energies and their correction, *Int. J. Chem. Kinet.*, *13*(9), 817–831, doi:10.1002/kin.550130906.

Hallquist, M., et al. (2009), The formation, properties and impact of secondary organic aerosol: current and emerging issues, *Atmos. Chem. Phys.*, *9*(14), 5155–5236, doi:10.5194/acp-9-5155-2009.

Hennigan, C. J., M. H. Bergin, A. G. Russell, A. Nenes, and R. J. Weber (2009), Gas/particle partitioning of water-soluble organic aerosol in Atlanta, *Atmos. Chem. Phys.*, *9*(11), 3613–3628, doi:10.5194/acp-9-3613-2009.

Hilal, S. H., S. W. Karickhoff, and L. A. Carreira (2003), Prediction of the vapor pressure boiling point, heat of vaporization and diffusion coefficient of organic compounds, *QSAR Comb. Sci.*, *22*(6), 565–574, doi:10.1002/qsar.200330812.

Hildebrandt, L., E. Kostenidou, N. Mihalopoulos, D. R. Worsnop, N. M. Donahue, and S. N. Pandis (2010), Formation of highly oxygenated organic aerosol in the atmosphere: Insights from the Finokalia Aerosol Measurement Experiments, *Geophys. Res. Lett.*, *37*, L23801, doi:10.1029/2010GL045193.

Hodzic, A., J. L. Jimenez, S. Madronich, M. R. Canagaratna, P. F. DeCarlo, L. Kleinman, and J. Fast (2010), Modeling organic aerosols in a megacity: Potential contribution of semi-volatile and intermediate volatility primary organic compounds to secondary organic aerosol formation, *Atmos. Chem. Phys.*, *10*(12), 5491–5514, doi:10.5194/acp-10-5491-2010.

Hoyle, C. R., et al. (2011), A review of the anthropogenic influence on biogenic secondary organic aerosol, *Atmos. Chem. Phys.*, *11*(1), 321–343, doi:10.5194/acp-11-321-2011.

Hu, K. S., A. I. Darer, and M. J. Elrod (2011), Thermodynamics and kinetics of the hydrolysis of atmospherically relevant organonitrates and organosulfates, *Atmos. Chem. Phys.*, *11*(16), 8307–8320, doi:10.5194/acp-11-8307-2011.

Huffman, J. A., et al. (2009), Chemically-resolved aerosol volatility measurements from two megacity field studies, *Atmos. Chem. Phys.*, *9*(18), 7161–7182, doi:10.5194/acp-9-7161-2009.

Jimenez, J. L., et al. (2009), Evolution of organic aerosols in the atmosphere, *Science*, *326*(5959), 1525–1529, doi:10.1126/science.1180353.

Koop, T., J. Bookhold, M. Shiraiwa, and U. Poschl (2011), Glass transition and phase state of organic compounds: dependency on molecular properties and implications for secondary organic aerosols in the atmosphere, *Phys. Chem. Chem. Phys.*, *13*(43), 19,238–19,255.

Kroll, J. H., N. L. Ng, S. M. Murphy, R. C. Flagan, and J. H. Seinfeld (2006), Secondary Organic Aerosol Formation from Isoprene Photooxidation, *Environ. Sci. Technol.*, *40*(6), 1869–1877, doi:10.1021/es0524301.

Kroll, J. H., J. D. Smith, D. L. Che, S. H. Kessler, D. R. Worsnop, and K. R. Wilson (2009), Measurement of fragmentation and functionalization pathways in the heterogeneous oxidation of oxidized organic aerosol, *Phys. Chem. Chem. Phys.*, *11*(36), 8005–8014.

Lee, B. H., et al. (2010), Measurement of the ambient organic aerosol volatility distribution: application during the Finokalia Aerosol Measurement Experiment (FAME-2008), *Atmos. Chem. Phys.*, *10*(24), 12149–12160, doi:10.5194/acp-10-12149-2010.

Lim, Y. B., and P. J. Ziemann (2005), Products and mechanism of secondary organic aerosol formation from reactions of n-alkanes with OH radicals in the presence of NOx, *Environ. Sci. Technol.*, *39*(23), 9229–9236, doi:10.1021/es051447g.

Lim, Y. B., Y. Tan, M. J. Perri, S. P. Seitzinger, and B. J. Turpin (2010), Aqueous chemistry and its role in secondary organic aerosol (SOA) formation, *Atmos. Chem. Phys.*, *10*(21), 10,521–10,539, doi:10.5194/acp-10-10521-2010.

Liu, S., et al. (2012a), Secondary organic aerosol formation from fossil fuel sources contribute majority of summertime organic mass at Bakersfield, *J. Geophys. Res.*, *117*, D00V26, doi:10.1029/2012JD018170.

Liu, S., J. E. Shilling, C. Song, N. Hiranuma, R. A. Zaveri, and L. M. Russell (2012b), Hydrolysis of organonitrate functional groups in aerosol particles, *Aerosol Sci. Technol.*, *46*(12), 1359–1369, doi:10.1080/02786826.2012.716175.

Matsunaga, A., and P. J. Ziemann (2008), Yields of Œ≤-hydroxynitrates and dihydroxynitrates in aerosol formed from OH radical-initiated reactions of linear alkenes in the presence of NOx, *J. Phys. Chem. A*, *113*(3), 599–606, doi:10.1021/jp807764d.

Ng, N. L., et al. (2007), Effect of NOx level on secondary organic aerosol (SOA) formation from the photooxidation of terpenes, *Atmos. Chem. Phys.*, *7*(19), 5159–5174, doi:10.5194/acp-7-5159-2007.

Ng, N. L., et al. (2008), Secondary organic aerosol (SOA) formation from reaction of isoprene with nitrate radicals (NO3), *Atmos. Chem. Phys.*, *8*(14), 4117–4140, doi:10.5194/acp-8-4117-2008.

Nguyen, T. B., J. Laskin, A. Laskin, and S. A. Nizkorodov (2011), Nitrogen-containing organic compounds and oligomers in secondary organic aerosol formed by photooxidation of isoprene, *Environ. Sci. Technol.*, *45*(16), 6908–6918, doi:10.1021/es201611n.

Nozière, B., I. Barnes, and K.-H. Becker (1999), Product study and mechanisms of the reactions of α-pinene and of pinonaldehyde with OH radicals, *J. Geophys. Res.*, *104*(D19), 23,645–23,656, doi:10.1029/1999JD900778.

O'Brien, R. E., A. Laskin, J. Laskin, S. Liu, R. Weber, L. M. Russell, and A. H. Goldstein (2013), Molecular characterization of organic aerosol using nanospray desorption/electrospray ionization mass spectrometry: CalNex 2010 field study, *Atmos. Environ.*, *68*(0), 265–272, doi:http://dx.doi.org/10.1016/j.atmosenv.2012.11.056.

Odum, J. R., T. Hoffmann, F. Bowman, D. Collins, R. C. Flagan, and J. H. Seinfeld (1996), Gas/particle partitioning and secondary organic aerosol yields, *Environ. Sci. Technol.*, *30*(8), 2580–2585, doi:10.1021/es950943+.

Pankow, J. F. (1994), An absorption model of gas/particle partitioning of organic compounds in the atmosphere, *Atmos. Environ.*, *28*(2), 185–188, doi:http://dx.doi.org/10.1016/1352-2310(94)90093-0.

Pankow, J. F., and W. E. Asher (2008), SIMPOL.1: A simple group contribution method for predicting vapor pressures and enthalpies of vaporization of multifunctional organic compounds, *Atmos. Chem. Phys.*, *8*(10), 2773–2796, doi:10.5194/acp-8-2773-2008.

Paulot, F., J. D. Crounse, H. G. Kjaergaard, J. H. Kroll, J. H. Seinfeld, and P. O. Wennberg (2009), Isoprene photooxidation: New insights into the production of acids and organic nitrates, *Atmos. Chem. Phys.*, *9*(4), 1479–1501, doi:10.5194/acp-9-1479-2009.

Perraud, V., et al. (2012), Nonequilibrium atmospheric secondary organic aerosol formation and growth, *Proc. Natl. Acad. Sci. U. S. A.*, *109*(8), 2836–2841.

Perring, A. E., S. E. Pusede, and R. C. Cohen (2013), An observational perspective on the atmospheric impacts of alkyl and multifunctional nitrates on ozone and secondary organic aerosol, *Chem. Rev.*, doi:10.1021/cr300520x.

Roberts, J. M. (1990), The atmospheric chemistry of organic nitrates, *Atmos. Environ.*, *24A*(2), 243–287.

Robinson, A. L., N. M. Donahue, M. K. Shrivastava, E. A. Weitkamp, A. M. Sage, A. P. Grieshop, T. E. Lane, J. R. Pierce, and S. N. Pandis (2007), Rethinking organic aerosols: Semivolatile emissions and photochemical aging, *Science*, *315*(5816), 1259–1262, doi:10.1126/science.1133061.

Rollins, A. W., et al. (2009), Isoprene oxidation by nitrate radical: Alkyl nitrate and secondary organic aerosol yields, *Atmos. Chem. Phys.*, *9*(18), 6685–6703, doi:10.5194/acp-9-6685-2009.

Rollins, A. W., J. D. Smith, K. R. Wilson, and R. C. Cohen (2010), Real time in situ detection of organic nitrates in atmospheric aerosols, *Environ. Sci. Technol.*, *44*(14), 5540–5545, doi:10.1021/es100926x.

Rollins, A. W., et al. (2012), Evidence for NOx control over nighttime SOA formation, *Science*, *337*(6099), 1210–1212, doi:10.1126/science.1221520.

Russell, L. M., R. Bahadur, and P. J. Ziemann (2011), Identifying organic aerosol sources by comparing functional group composition in chamber and atmospheric particles, *Proc. Natl. Acad. Sci. U. S. A.*, *108*(9), 3516–3521, doi:10.1073/pnas.1006461108.

Sprengnether, M., K. L. Demerjian, N. M. Donahue, and J. G. Anderson (2002), Product analysis of the OH oxidation of isoprene and 1,3-butadiene in the presence of NO, *J. Geophys. Res.*, *107*(D15), doi:10.1029/2001JD000716.

Surratt, J. D., et al. (2008), Organosulfate formation in biogenic secondary organic aerosol, *J. Phys. Chem. A*, *112*(36), 8345–8378, doi:10.1021/jp802310p.

Thornton, J. A., P. J. Wooldridge, and R. C. Cohen (2000), Atmospheric NO2: In situ laser-induced fluorescence detection at parts per trillion mixing ratios, *Anal. Chem.*, *72*(3), 528–539, doi:10.1021/ac9908905.

Weber, R. J., et al. (2007), A study of secondary organic aerosol formation in the anthropogenic-influenced southeastern United States, *J. Geophys. Res.*, *112*, D13302, doi:10.1029/2007JD008408.

Williams, B. J., A. H. Goldstein, N. M. Kreisberg, S. V. Hering, D. R. Worsnop, I. M. Ulbrich, K. S. Docherty, and J. L. Jimenez (2010), Major components of atmospheric organic aerosol in southern California as determined by hourly measurements of source marker compounds, *Atmos. Chem. Phys.*, *10*(23), 11,577–11,603, doi:10.5194/acp-10-11577-2010.

Wooldridge, P. J., et al. (2010), Total peroxy nitrates (ΣPNs) in the atmosphere: The thermal dissociation-laser induced fluorescence (TD-LIF) technique and comparisons to speciated PAN measurements, *Atmos. Meas. Tech.*, *3*(3), 593–607, doi:10.5194/amt-3-593-2010.

Zhang, H., J. D. Surratt, Y. H. Lin, J. Bapat, and R. M. Kamens (2011), Effect of relative humidity on SOA formation from isoprene/NO photooxidation: Enhancement of 2-methylglyceric acid and its corresponding oligoesters under dry conditions, *Atmos. Chem. Phys.*, *11*(13), 6411–6424, doi:10.5194/acp-11-6411-2011.

Zhang, H., et al. (2012), Organosulfates as tracers for secondary organic aerosol (SOA) formation from 2-methyl-3-buten-2-ol (MBO) in the atmosphere, *Environ. Sci. Technol.*, *46*(17), 9437–9446, doi:10.1021/es301648z.